



# Suction Stress of Clay Over a Wide Range of Saturation

Idil Deniz Akin · William J. Likos

Received: 13 June 2019 / Accepted: 1 August 2019 / Published online: 6 August 2019  
© Springer Nature Switzerland AG 2019

**Abstract** Quantifying the relationship between water retention and internal stress state of unsaturated soils has long been a challenge. Current effective stress formulations can effectively capture the relationship for coarse-grained soils, where capillary mechanisms dominate internal stress state over a wide range of saturation, but fail for fine-grained soils, particularly at low to intermediate saturation, where surface adsorption mechanisms dominate water retention and corresponding stress state. Internal stress state of compacted kaolinite specimens spanning saturation ( $S$ ) from 0 to 0.73 is measured through Brazilian tensile strength tests. Changes observed in strength, strain, and stiffness are analyzed to calculate evolution of internal stress with saturation. A model is proposed to quantify the relationship between water retention and internal stress for fine-grained and coarse-grained soils at saturations over the full range ( $0 \leq S \leq 1$ ). Performance of the model is evaluated by comparison with experimental results from the literature.

**Keywords** Unsaturated · Suction · Capillary · Adsorption · Effective stress · Kaolinite

## 1 Introduction

Soil mechanical behavior (e.g., strength, stiffness, volume change) is governed largely by the effective state of stress. Saturated soil behavior depends almost exclusively on Terzaghi's (1943) effective stress ( $\sigma'$ ) quantified as the difference between total stress ( $\sigma$ ), which is generally compressive, and pore water pressure ( $u_w$ ), which is also generally compressive for saturated soils ( $\sigma' = \sigma - u_w$ ). One of the primary advantages of Terzaghi's effective stress formulation is that a saturated soil–water system may be treated as a two-phase continuum with stresses  $\sigma$  and  $u_w$  defined and readily calculated or measured at the boundary level (e.g., Santamarina et al. 2001).

Unsaturated soils, on the other hand, are three-phase systems comprising solids (soil particles), liquid (pore water), and gas (pore air). The relative volume fraction, microstructure, and pressures of the pore water and air influence internal forces acting at particle–particle contacts and, consequently, the mechanical behavior of the soil system. Changes in relative volume fraction, microstructure, and fluid pressures may occur by wetting–drying and loading–unloading processes, and have a direct impact on interparticle forces and corresponding soil behavior.

---

I. D. Akin (✉)  
Department of Civil and Environmental Engineering,  
Washington State University, Pullman, WA 99164, USA  
e-mail: idil.akin@wsu.edu

W. J. Likos  
Department of Civil and Environmental Engineering,  
Geological Engineering Program, University of  
Wisconsin-Madison, Madison, WI 53706, USA  
e-mail: likos@wisc.edu

The relation between pore water retention and pore water potential, captured by the soil–water retention curve (SWRC), thus plays an essential role in defining the state of stress and mechanical behavior of unsaturated soils (e.g., Lu et al. 2010; Alonso et al. 1990).

To define the stress state, we refer to a notion similar to Terzaghi's effective stress for saturated soils, which includes skeletal forces that propagate through the solid matrix, but that also includes local internal forces concentrated at or near particle contacts (Lu and Likos 2006). Sources of these forces include physicochemical forces and cementation forces, which may each occur under either saturated or unsaturated conditions, as well as capillary forces, which are unique to unsaturated soils (e.g., Lu and Likos 2006; Akin and Likos 2017a; Sridharan and Rao 1973; Ingles 1962). Because the existence and magnitude of these internal forces depend on soil moisture, some researchers have sought to differentiate pore water in unsaturated soil into two regimes: adsorbed water at relatively low saturation and capillary water at relatively high saturation (e.g., Lu 2016; Lebau and Konrad 2010; Baker and Frydman 2009; Tuller et al. 1999; Zhou et al. 2016). The contribution of adsorbed water to soil water retention has been widely studied (e.g., Or and Tuller 1999; Zhou et al. 2016). However, adsorbed water has often been assumed to have no influence on effective stress (e.g., Konrad and Lebeau 2015; Zhou et al. 2016). Recent studies show that effective stress also changes with water content at very low saturation (Akin and Likos 2017a; Dong and Lu 2017). Effectively resolving stress state over a wide range of saturation thus requires that both adsorbed water and capillary water be considered in effective stress calculations.

Following the suction stress conceptualization of Lu and Likos (2006), effective stress ( $\sigma'$ ) for unsaturated (or saturated) soil is quantified as:

$$\sigma' = (\sigma - u_a) - \sigma^s \quad (1)$$

where  $\sigma$  is total stress,  $u_a$  is pore air pressure and  $\sigma^s$  is the suction stress characteristic curve (SSCC). The SSCC can be defined either as a function of suction ( $\psi$ ) or saturation ( $S$ ):

$$\sigma^s = -f(\psi) = -f(u_a - u_w) \quad (2a)$$

$$\sigma^s = -f(S) \quad (2b)$$

where  $f$  is a scaling function that quantifies the link between suction stress and either suction or saturation. Retaining the conventional soil mechanics sign convention, negative values of suction stress denote tensile internal stress and are additive with the total stress component in Eq. (1). Suction stress will thus generally increase the stiffness and strength of soil, or will contribute to a contractive volume change, as evident in a wide range of experimental studies (e.g., Fredlund and Morgenstern 1976; Cui and Delage 1996; Lu and Dong 2017).

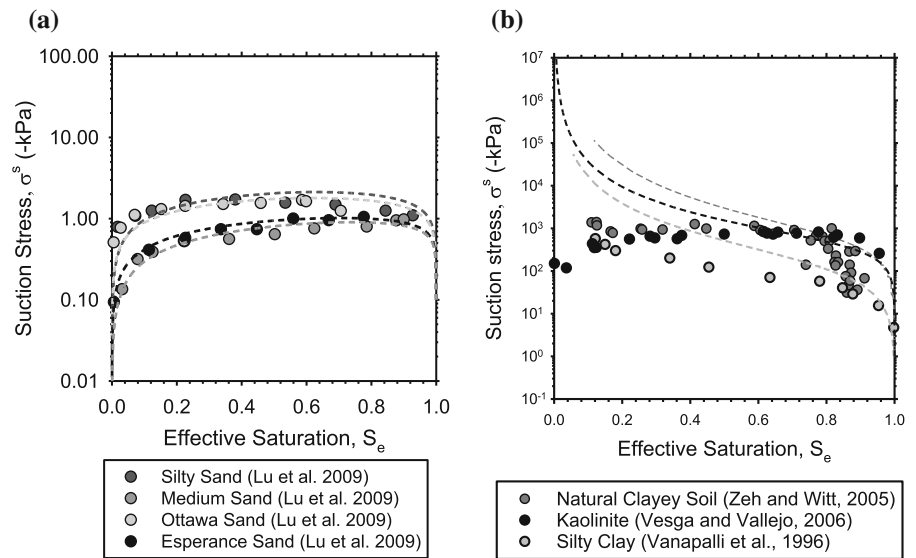
Equating the scaling function  $f$  in Eq. (2) to degree of saturation ( $S$ ) or effective degree of saturation ( $S_e$ ) is a commonly adopted approach [where  $S_e = (S - S_r)/(1 - S_r)$ ], and  $S_r$  is residual saturation determined by curve fitting to experimental SWRC data. This has some advantage because it leads to a convenient closed form equation for the SSCC (Lu et al. 2010), but does not effectively capture how adsorbed water contributes to internal stress, most notably for fine-grained soils where adsorbed water can be a significant fraction of total water retained.

The objective of this paper is to gain more comprehensive understanding of internal stress state for unsaturated soil over a wide range of saturation and to explore alternative scaling variables applicable for all soil types. Suction stress for a suite of compacted kaolinite specimens is quantified using Brazilian tensile strength (BTS) measurements (Akin and Likos 2017b). Changes observed in strength, strain, and stiffness of the specimens are analyzed to calculate the evolution of internal stress state with changing saturation. A new model is proposed to quantify the relationship between water retention and internal stress for fine-grained and coarse-grained soils for saturation over the full range ( $0 \leq S \leq 1$ ). Performance of the model is evaluated by comparison with experimental results for fine- and coarse-grained soils from the literature.

## 2 Background

Published results from tensile strength and shear strength experiments are shown in Fig. 1 to illustrate the shortcomings of using effective saturation ( $S_e$ ) as an effective stress scaling function. Figure 1a is a plot of SSCCs obtained from uniaxial tensile strength

**Fig. 1** Measured (symbols) and estimated (lines) suction stress characteristic curves of **a** sandy soils and **b** clayey soils by using  $\sigma^s = S_e \psi$ . Measured suction stress was back-calculated from uniaxial tensile strength measurements for sands and the kaolinite and clayey soil and from unconfined compressive strength tests for the silty clay



measurements for four different sands (Lu et al. 2009). In each case the SSCCs are non-monotonic functions characterized by zero suction stress at  $S_e = 0$ , zero suction stress at  $S_e = 1$ , and some peak suction stress at intermediate saturation. Solid lines are SSCCs directly calculated using water retention curves for the sands and  $S_e$  to link to suction to suction stress (i.e.,  $\sigma^s = -f(\psi) = -S_e \psi$ ). In each case  $S_e$  was determined by fitting the water retention curves for the sands using the van Genuchten (1980) model:

$$S_e = \frac{S - S_r}{1 - S_r} = \left[ \frac{1}{1 + (\alpha \psi)^n} \right]^m \tag{3}$$

where  $\alpha$ ,  $n$ , and  $m$  are fitting parameters. It is evident that the SSCCs determined experimentally are in good agreement with the calculated SSCCs over the entire range of saturation. These and other results indicate that scaling with effective saturation effectively accounts for capillary internal forces by volumetrically averaging the pore air and pore water pressure. It is also evident that short-ranged adsorption and physicochemical forces, which are not captured by averaging the fluid pressures, do not significantly contribute to internal stress and corresponding mechanical behavior of sands or other low plasticity soils dominated by capillary water retention (e.g., Pereira et al. 2010). Corresponding mechanical behavior of such materials (e.g., shear strength) can thus be effectively predicted by only considering capillary water (e.g., Zhou et al. 2016).

Figure 1b, is a plot of SSCCs for three clayey soils, including kaolinite (Vesga and Vallejo 2006), silty clay (Vanapalli et al. 1996), and a natural clayey soil (Zeh and Witt 2005). Measured suction stress (symbols) was back-calculated from uniaxial tensile strength measurements for the kaolinite and clayey soil, from triaxial shear strength tests for the recom-pacted expansive clay, and from unconfined compressive strength tests for the silty clay. Similar to Fig. 1a, the solid lines on Fig. 1b are SSCCs calculated using measured water retention curves and  $\sigma^s = -S_e \psi$  (i.e., fluid pressure averaging). Calculated suction stress is in this case zero at  $S_e = 1$ , increases as saturation decreases, and reaches some maximum at the dry or residual state. Suction stress measured directly from the soil mechanical response (symbols) compares well with the calculated SSCCs at high saturation, but deviates significantly at effective saturation as high as about 0.6–0.7. More examples on suction stress at low saturations can be found in Alsharif and McCartney (2014, 2015). This failure of the model suggests that capillary internal forces may dominate water retention of fine-grained soils at high saturation, but that internal forces resulting from short-ranged adsorption that become significant at intermediate saturation are not effectively accounted for with  $\sigma^s = -S_e \psi$ .

Ultimately, we propose that suction stress should be divided to differentiate a component due to adsorption ( $\sigma_a^s$ ) and a component due to capillarity ( $\sigma_c^s$ ):

$$\sigma^s(\psi) = \sigma_a^s(\psi) + \sigma_c^s(\psi) \tag{4}$$

While the capillary term may be effectively captured using the product  $-S_e\psi$ , there is currently no convenient or closed-form model for quantifying suction stress due to adsorption (i.e., the first term on the right-hand-side of Eq. (4) is poorly understood). Experiments herein were conducted to address this limitation by providing empirical evidence supporting a new SSCC model in the form of Eq. (4).

### 3 Materials and Methods

#### 3.1 Specimen Preparation

Suction stress characteristic curves for kaolinite clay were measured over a wide range of saturation using Brazilian tensile strength (BTS) tests following general procedures described by Akin and Likos (2017b). Kaolinite was specifically selected for this suite of tests because it is a low plasticity material, and thus is amenable to BTS testing, and because compacted BTS specimens consistently demonstrated a uniform splitting tensile failure mode confirmed by image analysis (Akin and Likos 2017b).

The kaolinite was obtained in powdered form and had specific gravity of 2.58. Specific surface area (SSA) estimated using a drying-based, single-point, water vapor adsorption method was  $12 \text{ m}^2/\text{g}$  (Akin and Likos 2016). Cation exchange capacity (CEC) measured by ammonium displacement was 5.5 meq/100 g. Additional index and mineralogy properties of the clay are summarized on Table 1.

Four different methods were used to precondition BTS specimens over a wide range of saturation. Two of the methods were vapor equilibration techniques adopted to capture the lower saturation range, where suction stress is predominantly controlled by adsorption and physicochemical forces. The third preparation method involved direct mixing of clay and liquid water and was used to target higher saturation, where capillary mechanisms dominate suction stress. A fourth method involved progressive drying of specimens from an initial slurry state and was used to capture potential effects of drying-induced cementation.

In the first approach, herein designated the “RH chamber” approach, oven-dried kaolinite powder ( $105 \text{ }^\circ\text{C}$ ) was compacted into a constant-volume mold

**Table 1** Index properties and mineralogy of kaolinite used in this study

SSA ( $\text{m}^2/\text{g}$ )	12
CEC (meq/100 g)	5.5
Specific gravity	2.58
*Particle size (% less than)	
5 $\mu\text{m}$	86
1 $\mu\text{m}$	60
0.5 micron	48
Median particle diameter ( $\mu\text{m}$ )	0.67
*Chemical analysis (%)	
SiO <sub>2</sub>	56.95
Al <sub>2</sub> O <sub>3</sub>	29.01
Fe <sub>2</sub> O <sub>3</sub>	0.88
TiO <sub>2</sub>	2.26
CaO	0.11
MgO	0.26
Na <sub>2</sub> O	0.08
K <sub>2</sub> O	0.69

to form disks with a specific, repeatable volume ( $V$ ). Disk dimensions were 3-cm in diameter ( $d$ ) and 1-cm in thickness ( $t$ ), such that  $V = 7.07 \text{ cm}^3$ . Compaction was achieved by applying a constant pressure of 552 kPa to the top platen of the specimen mold for 5 s. All specimens were prepared to void ratio of  $e = 1.01 \pm 0.01$ , which could be consistently achieved by placing exactly 9.1 g of dry clay into the mold and compacting each specimen to the same volume. Compacted specimens were extruded from the mold and placed in humidity-controlled chambers prepared using saturated solutions of six different salts: LiCl (11.3%  $R_H$ ), MgCl<sub>2</sub> (33.1%  $R_H$ ), Mg(NO<sub>3</sub>)<sub>2</sub> (52.9%  $R_H$ ), NaCl (75.5%  $R_H$ ), KCl (85.1%  $R_H$ ), and KNO<sub>3</sub> (93.6%  $R_H$ ), and an additional unsaturated Mg(NO<sub>3</sub>)<sub>2</sub> solution (82.0%  $R_H$ ). Specimens were kept in the RH chambers for 7 days to reach equilibrium and then tested for tensile strength. This approach produced a suite of 35 specimens ranging in final saturation from 0 to 0.07.

Following the second preparation approach, designated the “Auto-RH” approach, BTS disks were prepared by compacting oven-dried clay as described above, but then placing them in a conditioning chamber in which the relative humidity (RH) was maintained at approximately 99.9% using a mixed-

flow humidity control system (Likos and Lu 2002). Specimens were kept in the chamber for periods ranging from 7 to 45 days to equilibrate to an increasing range of water content. Corresponding total suction of the specimens after moisture conditioning was determined using a water potential meter incorporating the chilled-mirror dew point technique (WP4, METER Group, Inc., Pullman WA). Saturation was calculated from weight-volume relationships. This approach produced a suite of 21 specimens ranging in saturation from 0.10 to 0.28.

In the third approach, designated the “liquid water” approach, target saturation values were pre-selected. Oven-dried clay and deionized (DI) water were manually mixed in proportions to achieve target saturation at the same void ratio of  $1.01 \pm 0.01$ . Clay-water mixtures were mixed with a mortar and pestle to remove large clods and then compacted in the constant-volume mold following the same procedures as above. Corresponding suction of the specimens after compaction was measured using the water potential meter. This approach produced a suite of 21 specimens ranging in saturation from 0.02 to 0.73.

In the fourth approach, designated the “slurry” approach, kaolinite slurry was initially prepared at 85% gravimetric water content ( $w$ ) and placed directly in the compaction mold. Axial load was gradually applied to consolidate the specimens for 24 h. Compaction to  $e = 1.01 \pm 0.01$  was achieved following the approach previously described. The mold was kept in a sealed bag during consolidation and compaction to minimize moisture loss. Specimens were then air-dried to reach different saturations along a drying path and corresponding suction values were measured using the water potential meter. This approach produced a suite of 10 specimens ranging in saturation from 0.13 to 0.92.

### 3.2 Brazilian Tensile Strength (BTS) Testing

ASTM Standard D3967 describes testing apparatus, specimen preparation, and procedures for determining the splitting tensile strength of rock by diametral line compression of a disk-shaped specimen, an approach commonly known as the Brazilian tensile strength (BTS) test (e.g., Carneiro 1943; Hondros 1959). BTS tests were conducted according to procedures described in ASTM D3967, but using a reduced-scale apparatus (Fig. 2b) constructed for compatibility with

smaller loads and specimen sizes (Akin and Likos 2017b). Two different load cells were used. A micro, S-type load cell having 20 N capacity and 0.098 mN resolution was used for specimens prepared using the RH chamber, Auto-RH, and liquid water approaches, where applied forces were relatively low. A higher-capacity load cell was used (222 N capacity, 0.04 N resolution) for specimens prepared using the slurry approach because preliminary results showed that the capacity of the 20 N-load cell could be exceeded. In each case the load cell was attached to a stepper-motor-controlled load frame to apply compressive force to the specimens at a constant rate of displacement.

Two steel bearing blocks were constructed to have a  $14^\circ$  arc of contact with the 3-cm diameter disks. Curved bearing blocks were used to avoid local failure of the specimen edges and to ensure tensile failure along the specimen’s vertical diameter (Frydman 1964; Akin and Likos 2017b). Disks were placed on the bottom bearing block and compressive force was applied by imposing a constant displacement rate to the top bearing block. A suite of preliminary studies showed that displacement rate ranging from 0.10 to 1.0 mm/min did not significantly influence measured tensile strength (Akin and Likos 2017b). Accordingly, faster loading rates were used for specimens at higher saturations to reduce test time and minimize evaporative loss of water. For the RH chamber and Auto-RH specimens, a 0.25 mm/min loading rate was applied. For the liquid water specimens, a 0.25 mm/min loading rate was applied for specimens at  $S < 0.26$  and a 1 mm/min loading rate was applied at higher saturations. For slurry specimens, a 1 mm/min loading rate was applied. All specimens failed within 2 min using the 0.25 mm/min rate and within 1 min using the 1 mm/min rate.

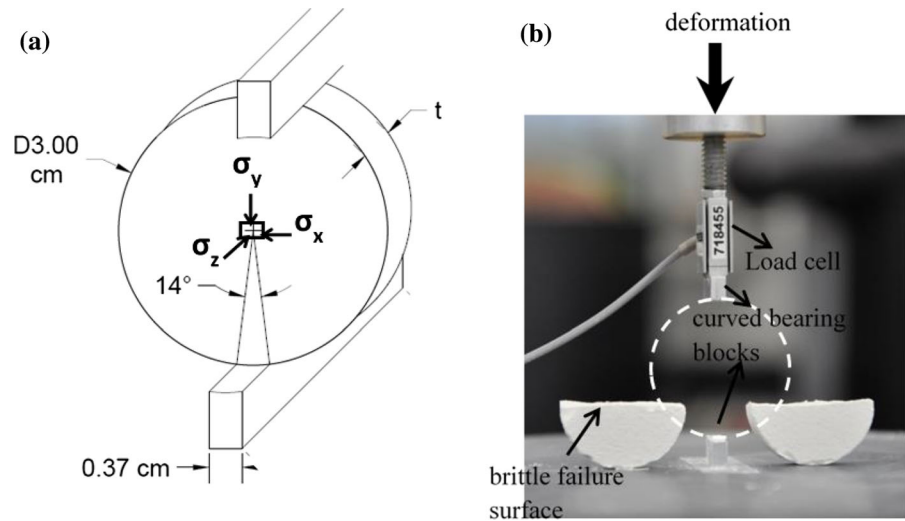
Applied force was continuously measured with the load cell at one-second intervals. Tensile strength ( $\sigma_t$ ) was calculated from applied compressive force at failure ( $P$ ) and the diameter ( $d$ ) and thickness ( $t$ ) of the specimen (Hondros 1959):

$$\sigma_x = \sigma_t = -\frac{2P}{\pi dt} \quad (5a)$$

with corresponding orthogonal stresses (Fig. 2a) for subsequent analysis of internal stress conditions at failure equal to:



**Fig. 2** Brazilian tensile strength (BTS) test for compacted kaolinite specimens: **a** specimen geometry; **b** post-test photograph of brittle tensile fracture



$$\sigma_y = -3\sigma_x = \frac{6P}{\pi dt} \tag{5b}$$

$$\sigma_z = 0 \tag{5c}$$

## 4 Results and Discussion

### 4.1 Soil Water Retention Curve (SWRC)

The soil–water retention curve (SWRC) for the kaolinite (Fig. 3) was obtained by combining results

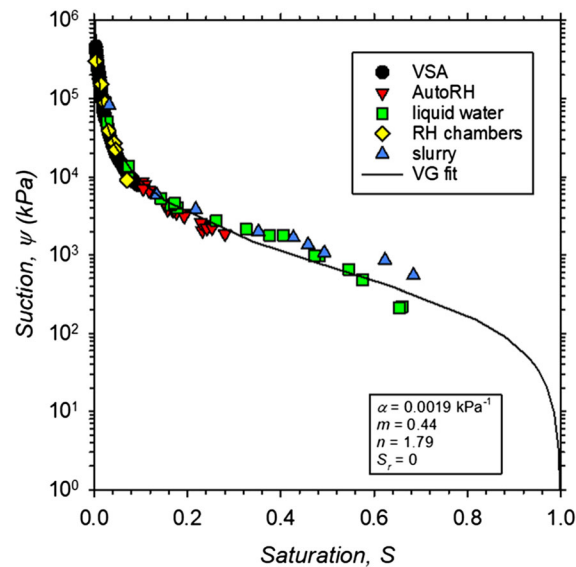


**Fig. 3** Suction stress characteristic curve of kaolinite

from the water potential meter measurements on BTS specimens and an independent sorption isotherm obtained using a vapor sorption apparatus (Meter Group, Pullman, WA) for the same clay in powdered form (Akin and Likos 2014). Water potential meter measurements were taken after each BTS test and are labeled separately on Fig. 3 to differentiate the four specimen preparation approaches. For specimens at  $S > 0.68$ , no suction measurement could be measured because the capacity of WP4 was exceeded. Results from the independent isotherm (denoted VSA) and BTS specimens conditioned by the RH chamber and Auto-RH procedures spanned the pendular water retention regime and the residual-to-funicular transition. Results for specimens conditioned by the liquid–water and slurry procedures spanned the widest range of saturation, up to a maximum of 0.68. At the highest saturations, the slurry method produced slightly higher suctions than the liquid water method. This difference is interpreted to reflect the effects of hydraulic hysteresis because specimens prepared using the slurry approach were conditioned along a drying path, whereas all other methods correspond to an initial wetting path. Close agreement among the methods at low saturation ( $S < 0.1$ ) indicates that variations in pore structure from the different specimen preparation approaches had little effect on water retention. This is attributed to the fact that water retention at high suction is dominated by surface adsorption mechanisms independent of the pore structure (e.g., Revil and Lu 2013; Frydman and Baker 2009).

The combined results define an SWRC spanning suction values from 470,000 kPa to 210 kPa and corresponding saturation from 0.3 to 68%. The solid line in Fig. 3 is a best-fit to the complete data set using the van Genuchten (1980) SWRC model (Eq. 3) for the wetting curve (i.e., slurry results were not used), with corresponding parameters  $\alpha = 0.0019 \text{ kPa}^{-1}$ ,  $m = 0.44$ ,  $n = 1.79$ , and  $S_r = 0$ .

Both WP4 and vapor sorption apparatus measure total suction, SWRC shown in Fig. 3 is in terms of total suction. Osmotic suction of kaolinite is assumed to be negligible for suction stress calculations (i.e., total suction was assumed to be equal to matric suction). Cation exchange capacity of the kaolinite was measured as 5.5 cmol +/kg by using the ammonium displacement method as describe in ASTM D7503, indicating that concentration of soluble cations is less than 1 cmol +/kg, and corresponding osmotic suction can be assumed negligible.

#### 4.2 Stress–Strain Response

Representative stress–strain response from BTS testing is shown in Fig. 4 in the form of tensile stress versus diametrical specimen strain. Tensile stress was quantified according to Eq. (5a) and diametrical strain ( $\varepsilon_d$ ) was quantified as the ratio of the change in vertical specimen diameter ( $\Delta d$ ) to its initial diameter ( $d$ ) of 3 cm. All specimens showed brittle failure along their vertical diameter at the right-most point on the stress–strain curves, but as saturation increased, the stress–strain response became progressively more ductile. Specimens took progressively larger deformations before failure and for the wettest specimen ( $S = 0.73$ ), deformation at failure was 0.185 cm. The BTS test is considered to accurately capture elastic behavior and tensile failure only if the ratio of the width of the flattened portion of the specimen edges under bearing plates ( $a$ ) to the vertical distance between flattened portions at failure ( $y$ ) does not exceed 0.27 (Frydman 1964). All specimens prepared by vapor equilibration had flattened edges over the entire width of the bearing blocks (0.366 cm) as observed by image analysis (Akin and Likos 2017b). For the wettest specimen that deformed 0.185 cm,  $a = 0.366$  and  $y = 2.63$  with corresponding ratio  $a/y = 0.14$ , which satisfies Frydman's (1964) criteria. The Auto-RH and liquid water specimens at  $S < \sim 0.50$  failed at  $\varepsilon_d$  ranging from approximately 1 to 2.5%. When saturation was

increased beyond 0.55,  $\varepsilon_d$  also increased, reaching 6.17 for the wettest (liquid water) specimens ( $S = 0.73$ ). The slurry specimens failed at approximately one order of magnitude higher tensile stresses and two times higher strains.

#### 4.3 Differences Resulting from Specimen Preparation

Figure 5 shows trends in tensile strength (Fig. 5a), diametrical strain at failure (Fig. 5b), and stiffness (Fig. 5c) with changing saturation. Specimen stiffness was obtained from the linear portion of the stress–strain curves. Stiffness calculated from BTS tests does not necessarily reflect the structural stiffness, but is a parameter that reflects the stress–strain relationship. To avoid the nonlinear portion of the stress–strain curve at small strains and for consistency, the portion between  $0.2 \varepsilon_{d,max}$  and  $0.8 \varepsilon_{d,max}$  was used, where  $\varepsilon_{d,max}$  is the diametrical strain at failure. Each aspect of behavior shown in Fig. 5 (strength, strain, stiffness) follows a similar trend with saturation, but there are two systematic offsets in the results: (1) there is an offset between results for specimens prepared using the vapor sorption-based approaches (i.e., RH chamber and Auto-RH) and the liquid–water approach, and (2) there is an offset in tensile strength and stiffness for specimens prepared using the slurry approach.

Specimens prepared using the liquid–water approach showed appreciably higher tensile strength and stiffness than the vapor sorption-based approaches at low saturations ( $S < 0.26$ ). This could be due to differences in soil fabric associated with compaction to different water contents (e.g., Mitchell et al. 1965). This discrepancy indicates that the liquid water method is not applicable for low saturations ( $S < 0.26$ ) because the amount of water is very small compared to the dry mass of soil (i.e.,  $w < 0.07$ ), which makes it very difficult to prepare a mixture with uniform moisture distribution. The recommended range for each specimen preparation technique is thus as follows: (1) RH chamber method for  $S < 0.07$ , (2) Auto-RH method for  $0.07 < S < 0.26$ , (3) liquid water method for  $S > 0.26$ , and (4) slurry method for the entire range of  $S$ . Figure 6 includes tensile strength results constrained within these ranges and is considered herein for analysis.

The slurry approach clearly gave higher tensile strength (approximately one order of magnitude

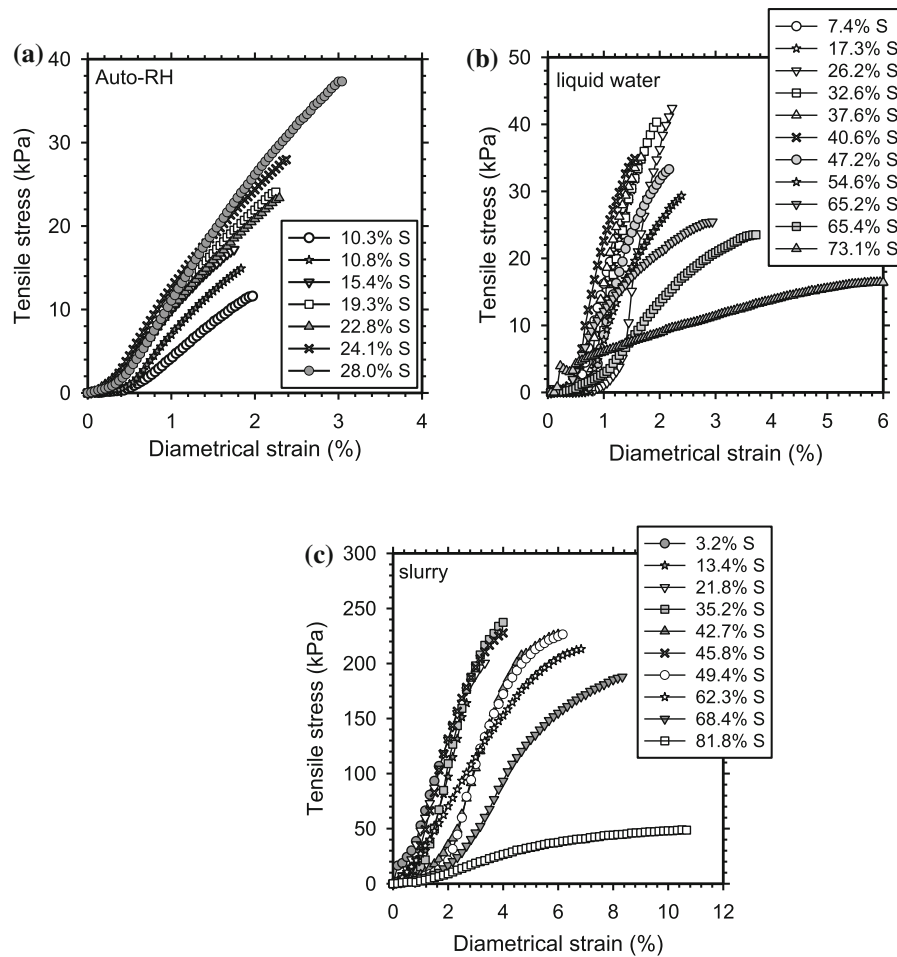


**Fig. 4** Stress strain response from BTS tests for **a** AutoRH, **b** liquid water, and **c** slurry specimens

higher) and stiffness (twice as high as the combined liquid water and sorption-based methods) results. Stronger and stiffer mechanical behavior is interpreted to indicate the effects of cementation forces resulting from drying from the initial slurry state. In general, cementation forces in saturated or unsaturated soils arise from covalent or ionic bonds formed between a cementing agent and soil particles. Such forces may arise from precipitation of dissolved solutes during a drying process, from other (e.g., microbially-induced) precipitation reactions (e.g., DeJong et al. 2006), or from migration of fines toward particle contacts during drying (e.g., Alramahi et al. 2010). Cementation increases the contact area between particles and consequently increases tensile strength (e.g., Fernandez and Santamarina 2001). Cementation forces depend on the strength of the cement, strength of the

individual particles, and strength of the cement-particle interface (Mitchell and Soga 2005). Ingles (1962) estimated an upper bound of about 300 kPa for the magnitude of internal cementation stress in soils. In the slurry method, during the drying process finer soil particles or salts that naturally exist in the soil might have migrated and precipitated at particle contacts, increasing the strength and stiffness of the specimens.

#### 4.4 Tensile Strength, Diametrical Strain, and Stiffness

Trends in tensile strength, diametrical strain, and stiffness with saturation can be interpreted by considering the evolution of internal stress with saturation. General trends in mechanical properties with



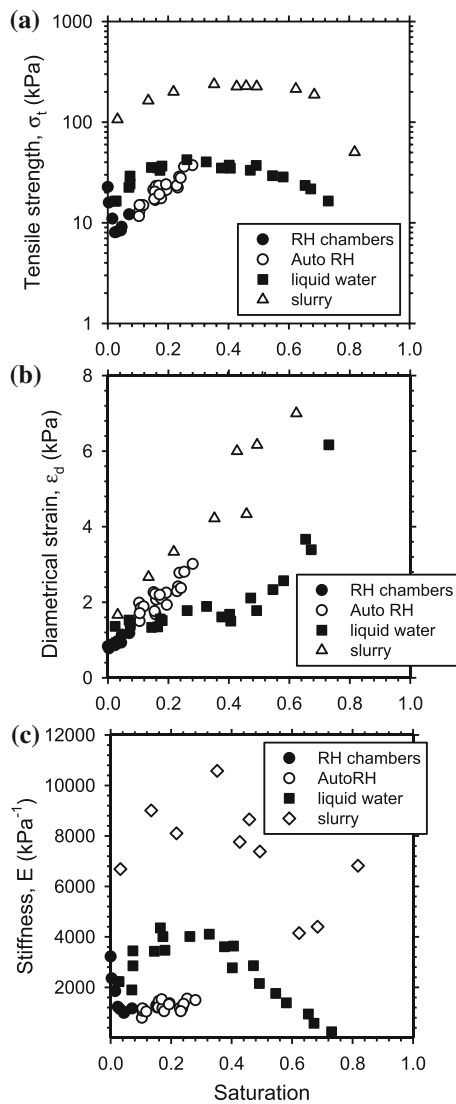


**Fig. 5** Results from BTS tests: tensile strength (a), strain at failure (b), and stiffness (c)

saturation are comparable, regardless of the differences induced by specimen preparation method. For tensile strength, the combined results from the vapor sorption-based and liquid water methods (Fig. 6) will be used for discussion. For discussion on diametrical strain and stiffness, Fig. 5b, c will be used, respectively. The slurry specimens showed similar trends in tensile strength, diametrical strain, and stiffness with saturation, but further discussion in this section will exclude slurry specimens due to the confounding effects of cementation.

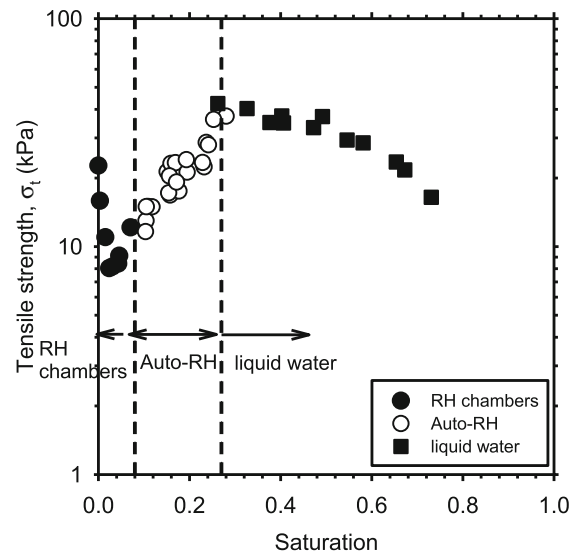


**Fig. 6** Complete SSCC of kaolinite and recommended ranges for each specimen preparation technique

As evident on Fig. 6, tensile strength of the kaolinite disks initially decreased from 22.7 kPa at  $S = 0$  (oven-dry), to 8.4 kPa at  $S \sim 0.04$ . Further increase in saturation caused an increase in tensile strength, reaching a peak of 40.4 kPa at  $S \sim 0.3$ , followed by a subsequent decrease. The wettest specimen ( $S = 0.73$ ) had tensile strength of 16.5 kPa. The initial decrease and subsequent increase can be attributed to a decrease in attractive van der Waals forces as the particles initially hydrate and the start of capillary condensation. Transition between a surface-dominated water retention regime and a capillary-dominated water retention regime may be defined as the residual transition (Akin and Likos 2017a). The decrease in tensile strength beyond around  $S = 0.3$  can be because of the combined effect of increasing double layer repulsive forces and diminishing capillary forces. When the double layers of two charged surfaces overlap, repulsive particle–particle forces develop that cause repulsive internal stress (e.g., van Olphen 1991; Mitchell and Soga 2005). The magnitude of the double layer forces is greatest for clays saturated with water and decreases exponentially as saturation decreases. The decrease in tensile strength for the kaolinite is interpreted to reflect the diminishing capillary forces. The contribution of capillary forces to internal stress gradually disappears with the loss of liquid bridges at higher saturations.

The change in internal stress components affected failure strain (Fig. 5b) and stiffness (Fig. 5c) in a similar manner. Diametrical strain was the smallest at oven-dried (105 °C) condition and gradually increased with saturation. Stiffness showed a similar trend as tensile strength, a decrease in stiffness after oven-dried condition was followed by an increase that reaches a peak, and a decrease as 100% saturation was reached.

#### 4.5 Suction Stress Characteristic Curve (SSCC)

The suction stress characteristic curve (SSCC) for the kaolinite can be back-calculated from the tensile strength results in  $p'$ - $q$  space. Mean total stress ( $p$ ) and deviatoric stress ( $q$ ) for a BTS specimen may be calculated as (Li et al. 2015):

$$p = \frac{1}{3}(\sigma_x + \sigma_y + \sigma_z) \tag{6a}$$

$$q = \frac{1}{\sqrt{2}}\sqrt{(\sigma_y - \sigma_z)^2 + (\sigma_y - \sigma_x)^2 + (\sigma_z - \sigma_x)^2} \tag{6b}$$

where  $\sigma_x$ ,  $\sigma_y$ , and  $\sigma_z$  for a BTS specimen at failure were previously defined by Eqs. (5a), (5b), and (5c), respectively. Mean effective stress ( $p'$ ) within the Lu and Likos (2006) suction stress framework is thus:

$$p' = p - \sigma^s = \frac{1}{3}(\sigma_x + \sigma_y + \sigma_z) - \sigma^s \tag{7}$$

where  $\sigma^s$  is the prevailing suction stress at failure. If the critical state friction angle  $\phi^{cs}$  of the clay is assumed to be independent of saturation or matric suction, as shown in previous studies (e.g., Escario 1980; Lu and Likos 2004), then a linear failure envelope may be plotted in  $p'$ - $q$  space with slope  $m$ , where:

$$m = \frac{6 \sin \phi^{cs}}{3 - \sin \phi^{cs}} \tag{8}$$

Suction stress of the compacted kaolinite disks calculated using Eqs. (7) and (8) are shown as symbols in Fig. 7. An internal friction angle for kaolinite of 24° was adopted for the analysis.

#### 4.6 Conceptual Model for SSCC

The mechanisms that contribute to suction stress are physicochemical forces that include van der Waals

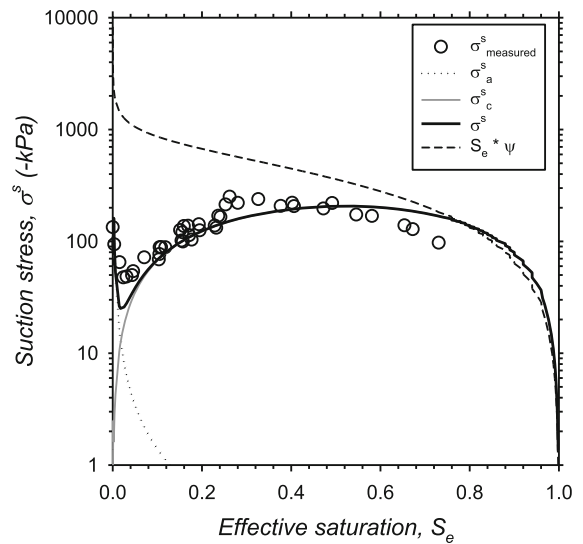


**Fig. 7** Measured (symbols) and calculated (solid black line) SSCC, and internal stress components (dotted line and grey line respectively for adsorption and capillarity) of kaolinite

forces and double layer forces, cementation forces, and capillary forces that arise from matric suction and surface tension at air–water interfaces (Lu and Likos 2006). The conceptual models for suction stress components were proposed by Lu and Likos (2006) and Akin and Likos (2017a, b) indicate that SSCC is a non-monotonic function of saturation (or suction) dominated by adsorptive forces at low saturations, and capillary forces at high saturations. For clayey soils, physicochemical forces result in a some value of suction stress that initially decreases with saturation and increases after retention mechanism transitions from adsorption-dominated to capillarity-dominated, and decreases with the loss of capillary forces as saturation increases further.

#### 4.7 Proposed Model for SSCC

Based on the conceptual model, a mathematical model was developed from the experimental results by superimposing the adsorption ( $\sigma_a^s$ ) and capillary ( $\sigma_c^s$ ) components of SSCC as: The adsorption-dominated regime and capillarity-dominated regime of both SSCC and SWRC were treated separately in the form:

$$\sigma^s(\psi) = \sigma_a^s(\psi) + \sigma_c^s(\psi) \tag{9a}$$

The adsorption component normalizes the suction stress at oven-dry (105 °C) conditions ( $\sigma_{dry}^s$ ) and

suction at any saturation with  $10^6$  kPa, which is the theoretical maximum suction, and has the form:

$$\sigma_a^s = \left(\frac{\psi}{10^6}\right) \times \sigma_{dry}^s \tag{9b}$$

The capillary component normalizes effective saturation with effective saturation at air entry pressure ( $S_{e,ae}$ ) and uses an exponential function that normalizes air entry pressure ( $\psi_{ae}$ ) with suction at any saturation value.  $\sigma_c^s$  is the product of this exponential function with suction, and normalized saturation, and has the form:

$$\sigma_c^s = \left(\frac{\psi_{ae}}{\psi_{ae} + \psi}\right) \times \psi \times \left(\frac{S_e}{S_{e,ae}}\right) \tag{9c}$$

Both  $\psi_{ae}$  and  $S_{e,ae}$  are determined using Van Genuchten (1980) Model.

The model requires measurements of suction stress at dry conditions and soil water retention curve. Figure 7 shows the performance of the proposed model fit to the measured SSCC data for the kaolinite and independently plots the adsorption and capillary term. The adsorption term has a maximum value at 0 effective saturation and decreases exponentially as  $S_e$  increases. The capillary term is zero at  $S_e = 0$  and  $S_e = 1$ , and reaches a maximum value at approximately  $S_e = 0.4$ . The resultant SSCC follows the same trend as the measured data, characterized by an initial decrease as  $S_e$  increases from fully dry conditions to approximately  $S_e = 0.04$ , followed by an increase and decrease after reaching a maximum at around  $S_e = 0.4$ . By comparison, the SSCC in the form  $\sigma^s = -S_e\psi$  (also plotted on Fig. 7) performs very poorly.

More general performance of the proposed model was evaluated using the soils in Fig. 1b. Figure 8 compares the proposed model and  $\sigma^s = -S_e\psi$ . For all three soils, the SSCC in the form  $\sigma^s = -S_e\psi$  provides a reasonable match to the experimental data only for high saturations, whereas the proposed model successfully estimates the SSCC behavior over the entire range of saturation.

### 5 Conclusions

Internal stress of compacted kaolinite disks was measured through a series of Brazilian tensile strength (BTS) tests. Specimens were equilibrated to

saturations ranging from 0 to 0.73 using four different hydration techniques: (1) equilibrating disks in saturated salt solution chambers, (2) equilibrating disks in a closed chamber for various lengths of time at nearly 100% RH, (3) mixing dry kaolinite with water at target saturations, and (4) drying the disks from an initial slurry form. Evolution in strength, strain, and stiffness of the disks with increasing saturation was evaluated to clarify dominant internal stress components and to propose a new scaling function that quantifies the relationship between suction stress and saturation. The new model explicitly differentiates suction stress arising from adsorption effects and suction stress arising from capillary effects. The following observations, conclusions, and recommendations can be made:

- Three different hydration techniques are recommended to be used concurrently to reach saturations in the entire range for a wetting-based approach to measure SSCC. Sorption-based methods (i.e., RH chamber and Auto-RH) are recommended for low saturations, where adsorption dominates water uptake, and direct mixing of soil with liquid water (i.e., liquid water method) is recommended at higher saturations, where capillarity dominates water uptake. For the kaolinite used in the current suite of tests, these ranges were  $S < 0.07$  for RH chamber method,  $0.07 < S < 0.26$  for Auto-RH method, and  $S > 0.26$  for liquid water method. Alternatively, for a drying-based approach to measure SSCC slurry method is recommended for the entire range of  $S$ .
- A drying-based method to prepare specimens induces cementation that results in an order of magnitude higher tensile stresses and two times higher strains.
- Suction stress of the disks at failure was calculated from the tensile strength measurements. Suction stress initially decreased from  $S = 0$  to approximately  $S = 0.04$  because of the decrease in attractive van der Waals forces, started to increase with the start of capillary forces and reached a peak at approximately  $S = 0.3$ , and started to decrease with the decreasing capillary forces, eventually reaching zero.
- Quantifying suction stress as the product of effective saturation and matric suction, which

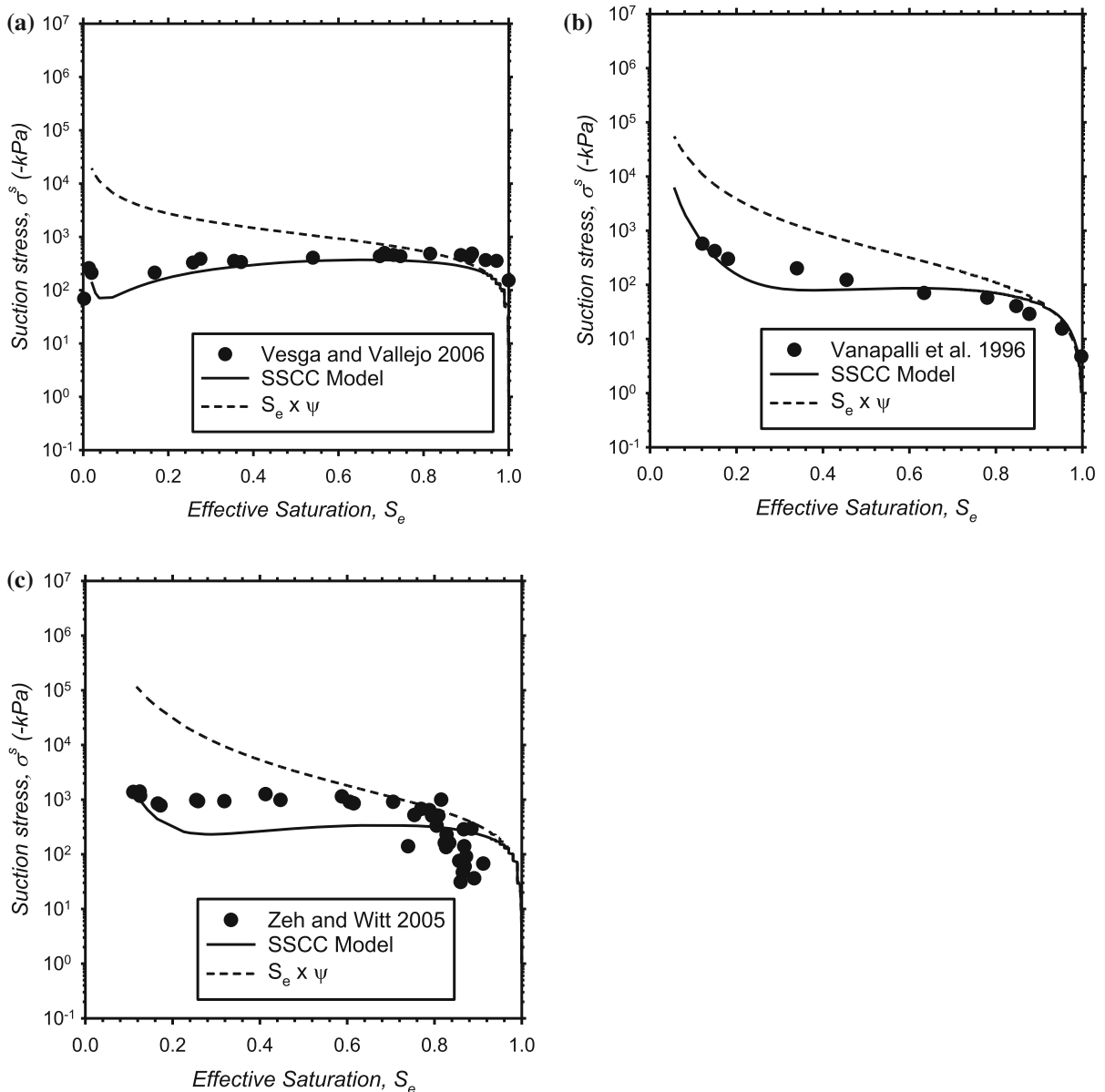


**Fig. 8** Performance of the proposed model to estimate SSCC of fine-grained soils

disregards the adsorption component of suction stress fails for fine-grained soils. A new equation was developed that explicitly considers both adsorption and capillary components of suction stress. The new model appears to effectively capture the relationship between the SWRC and the SSCC over the entire saturation range.

**Acknowledgements** This material is based on work supported by the National Science Foundation (NSF) under Grant CMMI

1304119. Any opinions, findings, and conclusions or recommendations are those of the authors and do not necessarily reflect the views of NSF.

## References

Akin ID, Likos WJ (2014) Specific surface area of clay using water vapor and EGME sorption methods. *Geotech Test J* 37(6):1–12

- Akin ID, Likos WJ (2016) Single-point and multi-point water-sorption methods for specific surface areas of clay. *Geotech Test J*. <https://doi.org/10.1520/gtj20150117>
- Akin ID, Likos WJ (2017a) Implications of surface hydration and capillary condensation to strength and stiffness of compacted clay. *J Eng Mech*. [https://doi.org/10.1061/\(asce\)em.1943-7889.0001265](https://doi.org/10.1061/(asce)em.1943-7889.0001265)
- Akin ID, Likos WJ (2017b) Brazilian tensile strength testing of compacted clay. *Geotech Test J*. <https://doi.org/10.1520/gtj20160180>
- Alonso EE, Gens A, Josa A (1990) A constitutive model for partially saturated soils. *Géotechnique* 40(3):405–430
- Alramahi BA, Alshibli KA, Fratta D (2010) Effect of fine particle migration on the small-strain stiffness of unsaturated soils. *J Geotech Geoenviron Eng* 136(4):620–628
- Alsherif N, McCartney JS (2014) Effective stress in unsaturated silt under low degrees of saturation. *Vadose Zone J* 13(5):1–13. <https://doi.org/10.2136/vzj2013.06.0109>
- Alsherif NA, McCartney JS (2015) Nonisothermal behavior of compacted silt at low degrees of saturation. *Géotechnique* 65(9):703–716
- ASTM D3967-08 (2008) Standard test method for splitting tensile strength of intact rock core specimens. ASTM International, West Conshohocken
- Baker R, Frydman S (2009) Unsaturated soil mechanics: critical review of physical foundations. *Eng Geol* 106:26–39
- Carneiro F (1943) A new method to determine the tensile strength of concrete. In: Proceedings of the 5th meeting of the Brazilian Association for technical rules, Sao Paulo, Brazil, September 16, The Brazilian Association of Technical Norms (ABNT), Sao Paulo, Brazil, pp 126–129
- Cui J, Delage P (1996) Yielding and plastic behavior of an unsaturated compacted silt. *Géotechnique* 46(2):291–311
- De Jong JT, Fritzes MB, Nüsslein K (2006) Microbially induced cementation to control sand response to undrained shear. *J Geotech Geoenviron Eng* 132(11):1381–1392
- Dong Y, Lu N (2017) Measurement of suction-stress characteristic curve under drying and wetting conditions. *Geotech Test J* 40(1):107–121
- Escario V (1980) Suction-controlled penetration and shear tests. In: Proceedings of the 4th international conference on expansive soils, Denver, pp 781–787
- Fernandez AL, Santamarina JC (2001) Effect of cementation on the small-strain parameters of sands. *Can Geotech J* 38:191–199
- Fredlund DG, Morgenstern NR (1976) Constitutive relations for volume change in unsaturated soils. *Can Geotech J* 13:261–276
- Frydman S (1964) The applicability of the Brazilian (indirect tension) test to soils. *Aust J Appl Sci* 15(4):335–343
- Frydman S, Baker R (2009) Theoretical soil–water characteristic curves based on adsorption, cavitation, and a double porosity model. *Int J Geomech* 9(6):250–257
- Hondros G (1959) The evaluation of Poisson's ratio and the modulus of materials of a low tensile resistance by the Brazilian (indirect tensile) test with particular reference to concrete. *Aust J Appl Sci* 10(3):243–268
- Ingles OG (1962) A theory of tensile strength for stabilized and naturally coherent soils. In: Proceedings of the 1st conference of the Australian Road Research Board, vol 1, pp 1025–1047
- Konrad J-M, Lebeau M (2015) Capillary-based effective stress formulation for predicting shear strength of unsaturated soils. *Can Geotech J*. <https://doi.org/10.1139/cgj-2014-0300>
- Lebeau M, Konrad J-M (2010) A new capillary and thin film flow model for predicting the hydraulic conductivity of unsaturated porous media. *Water Resour Res* 46:W12554
- Li X, Wen H, Muhunthan B, Wang J (2015) Modeling and prediction of the effects of moisture on the unconfined compressive and tensile strength of soils. *J Geotech Geoenviron Eng* 141(7):04015028
- Likos WJ, Lu N (2002) Water-vapor sorption behavior of smectite-kaolinite mixtures. *Clays Clay Miner* 50(5):553–561
- Lu N (2016) Generalized soil water retention equation for adsorption and capillarity. *J Geotech Geoenviron Eng*. [https://doi.org/10.1061/\(asce\)gt.1943-5606.0001524](https://doi.org/10.1061/(asce)gt.1943-5606.0001524)
- Lu N, Dong Y (2017) Correlation between soil-shrinkage curve and water-retention characteristics. *J Geotech Geoenviron Eng* 143(9):04017054
- Lu N, Likos WJ (2004) *Unsaturated soils mechanics*. Wiley, New York
- Lu N, Likos WJ (2006) Suction stress characteristic curve for unsaturated soil. *J Geotech Geoenviron Eng* 132(2):131–142
- Lu N, Kim T-H, Sture S, Likos WJ (2009) Tensile strength of unsaturated sand. *J Eng Mech* 135:1410–1419
- Lu N, Godt JW, Wu DT (2010) A closed-form equation for effective stress in unsaturated soils. *Water Resour Res*. <https://doi.org/10.1029/2009wr008646>
- Mitchell JK, Soga K (2005) *Fundamentals of soil behavior*, 3rd ed. Wiley, Hoboken
- Mitchell JK, Hooper DR, Campanella RG (1965) Permeability of compacted clay. *J Soil Mech Found Div ASCE* 91(SM4):41–65
- Pereira JM, Coussy O, Alonso EE, Vaunat J, Olivella S (2010) Is the degree of saturation a good candidate for Bishop's parameter? In: Alonso EE, Gens A (eds) *Unsaturated soils—proceedings of 5th international conference on unsaturated soils*, vol 2. CRC Press, Barcelona, pp 913–919
- Revil A, Lu N (2013) Unified water isotherms for clayey porous materials. *Water Resour Res* 49:5685–5699
- Santamarina JC, Klein KA, Fam MA (2001) *Soils and waves*. Wiley, New York
- Sridharan A, Rao VG (1973) Mechanisms controlling volume change of saturated clays and the role of the effective stress concept. *Géotechnique* 23(3):359–382
- Terzaghi K (1943) *Theoretical soil mechanics*. Wiley, New York
- Tuller M, Or D, Dudley LM (1999) Adsorption and capillary condensation in porous media: liquid retention and interfacial configurations in angular pores. *Water Resour Res* 35(7):1949–1964
- van Genuchten MT (1980) A closed form equation for predicting the hydraulic conductivity of unsaturated soils. *Soil Sci Soc Am J* 44:892–898
- van Olphen H (1991) *Clay colloid chemistry*, 2nd edn. Krieger, Berlin
- Vanapalli S, Fredlund D, Pufahl D, Clifton A (1996) Model for the prediction of shear strength with respect to soil suction. *Can Geotech J* 33:379–392



- Vesga LF, Vallejo LE (2006) Direct and indirect tensile test for measuring the equivalent effective stress in a kaolinite clay. In: Unsaturated soils 2006, ASCE, pp 1290–1301
- Zeh RM, Witt KJ (2005) Suction-controlled tensile strength of compacted clays. In: Proceedings of the 16th international conference on soil mechanical geotechnical engineering, vol 4, Osaka, Japan, pp 2347–2352
- Zhou A, Huang R, Sheng D (2016) Capillary water retention curve and shear strength of unsaturated soils. *Can Geotech J* 53(6):974–987

**Publisher's Note** Springer Nature remains neutral with regard to jurisdictional claims in published maps and institutional affiliations.